International Journal of Solids and Structures 48 (2011) 1466–1473

Contents lists available at ScienceDirect

International Journal of Solids and Structures

journal homepage: www.elsevier.com/locate/ijsolstr

Model for thermoelastic actuation of an axisymmetric isotropic circular plate via an internal harmonic heat source ☆

Benjamin A. Griffin [a,1,2], Venkataraman Chandrasekaran [b], Matthew D. Williams [a,1,2], Bhavani V. Sankar [a], Mark Sheplak [a,*,2]

[a] Department of Mechanical and Aerospace Engineering, University of Florida, Gainesville, FL 32611, USA
[b] Analog Devices Inc., 804 Woburn St., MS-115, Wilmington, MA 01887-3494, USA

ARTICLE INFO

Article history:
Received 15 January 2010
Received in revised form 11 October 2010
Available online 2 February 2011

Keywords:
Proximity sensor
Plate
Thermoelastic
MEMS

ABSTRACT

This paper presents a reduced analytical modeling method for the initial optimal design of thermoelastic micromachined actuators. The key aspects of the model are a Green's function formulation of the axisymmetric heat conduction equation that incorporates an internal heat source and the solution of the thermoelastically forced bending wave equation. Model results of a representative thermoelastic structure include transient temperature and sinusoidal steady state transverse displacement. Comparison with finite element analysis shows excellent agreement with favorable computational costs. Model constraints at low frequencies are identified and discussed. The computational efficiency of the analytical model makes it a more viable modeling method for design optimization.

1. Introduction

Thermoelastic actuation of plates and beams has proven to be a viable actuation mechanism for micromachines (Lammerink et al., 1990; Popescu et al., 1996; Brand et al., 1997; Hornung and Brand, 1999; Rufer et al., 2006). Thermoelastic devices utilize Joule heating in a resistive element to generate a spatially non-uniform temperature field and hence non-uniform thermal expansion. The results are thermal force and moment resultants that cause deflections of structures such as beams and plates. In many cases, the deflection is enhanced by the non-uniform thermal expansion coefficients of composite structures (Chandrasekaran et al., 2003; Paul and Baltes, 1999).

A common characteristic of thermomechanical devices is the substantial design space. Device parameters include structural geometry, such as plate radius and thickness, as well as heater geometry. Typically, the devices are laminated composite structures, which introduces layer thicknesses as another design variable. The heater formation may also increase design complexity by adding new variables such as doping concentration for implanted resistors. Because of the broad design space, design optimization is best suited to select the proper combination of design variables for superior device performance. Finite element analysis (FEA) proves computationally costly for design optimization because of the large number of design variables. Therefore, an analytical model with low computational cost is desirable for design optimization of themoelastic micromachines.

Analytical solutions for thermoelastic vibration of beams and plates are prevalent in the literature. Lammerink et al. (1990, 1991, 1992) analytically treated a homogeneous silicon beam thermoelastically forced by a sheet source that simulated a film resistor heater on the top surface. Heat conduction along the beam was not taken into account. They also considered a distributed source within the beam under similar assumptions. Paul and Baltes (1999) analyzed a 1-D clamped composite plate in Cartesian coordinates with a heating resistor. Their thermal model separated the plate into two sections. The inner section was assumed to have a uniform temperature field created by the heater. The outer section was assumed to maintain the ambient temperature. This created an infinite temperature gradient at the heater edge which caused over-prediction of the thermal forcing function. Irie and Yamada (1978) studied the vibration of circular and annular plates with sinusoidally varying heat flux on one surface and thermal insulation on the other. The temperature in this study was assumed to be uniform in the radial direction due to the large aspect ratio. Prasanna and Spearing (2007) modeled thermoelastic cantilever beam vibrations using thermal lumped elements to approximate heat transfer within the beam and calculate the thermal moment.

☆ This work was supported by the Office of Naval Research.
* Corresponding author. Tel.: +1 3522819280; fax: +1 3523927303.
E-mail address: sheplak@ufl.edu (M. Sheplak).
[1] The work of M. Williams and B. Griffin was supported by the National Science Foundation.
[2] B. Griffin, M. Williams, and M. Sheplak are with the Interdisciplinary Microsystems Group at the University of Florida.

0020-7683/$ - see front matter © 2011 Elsevier Ltd. All rights reserved.
doi:10.1016/j.ijsolstr.2011.01.029

The thermal wavelength had to be much larger than the lumped elements for model accuracy. At high frequencies, the thermal wavelengths become smaller than the structure, requiring the density of elements within the beam or plate to increase for model accuracy.

The goal of the current study is to formulate a simplified analytical model of the thermoelastic actuation of the micromachined ultrasonic proximity sensor (Chandrasekaran et al., 2002) shown in Fig. 1. The analytical model will accurately describe device performance while minimizing computational cost for design optimization. Furthermore, an analytical solution provides scaling relations from which critical parameters in the design are identified.

The ultrasonic proximity sensor (Chandrasekaran et al., 2002) consists of a circular composite diaphragm with an axisymmetric heater for actuation. The heater consists of two semicircular diffused resistive elements. The diaphragm also contains arc and tapered piezoresistors (Campbell, 2001) for ultrasonic sensing (Chandrasekaran et al., 2002) which are not treated in the current study. The first level of actuation modeling of the device is the analytical solution of the equations of motion for an isotropic, silicon plate subject to homogeneous boundary conditions. The plate motion is governed by the axisymmetric bending wave equation under thermal forcing due to a non-uniform temperature distribution. The axisymmetric heat conduction equation with heat generation governs the non-uniform temperature field. The heater is modeled as a single, internal 2-D harmonic source. The radial and transverse thermal gradients couple into the thermal forcing term in the bending wave equation.

This paper is organized as follows. The bending wave equation under thermal forcing is derived in Section 2. The temperature field is found using Green's functions in Section 3. In Section 4 the bending wave equation is solved after incorporating the temperature field solution. In Section 5 results, including temperature distribution and deflection mode shapes, are presented and scaling parameters are discussed. Concluding remarks are contained in Section 6.

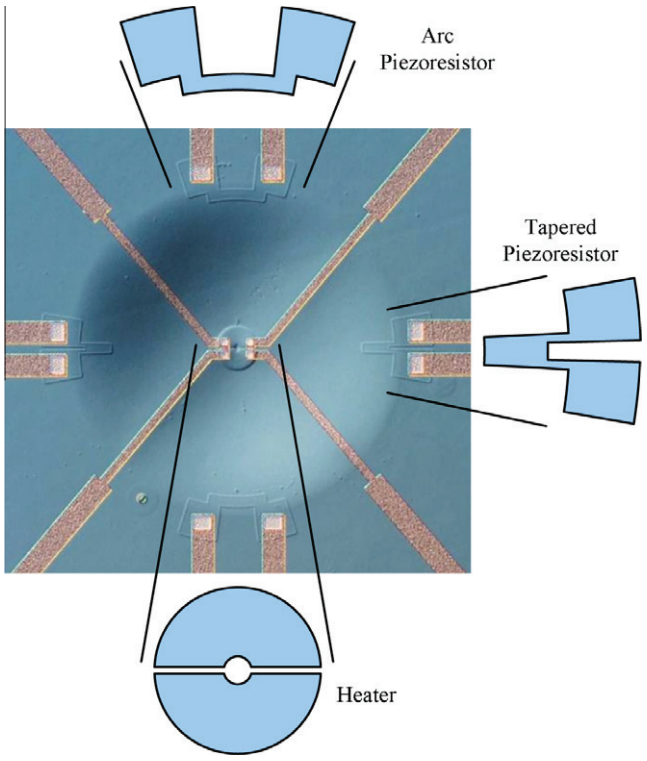

Fig. 1. The micromachined ultrasonic proximity sensor contains a Wheatstone bridge of two pairs of diffused arc and tapered piezoresistors for sensing. Two semicircles form the diffused resistive heater.

2. Mechanical formulation

In this section, the axisymmetric bending wave equation of an isotropic plate under thermoelastic loading from an arbitrary temperature field is derived. The derivation assumes that Kirchhoff's hypothesis is valid (Reddy, 1999). The cross-section of the axisymmetric circular plate with internal heat source is shown in Fig. 2.

2.1. Dynamic equilibrium

The equations of motion for an axisymmetric, circular plate are (Reddy, 1999):

$$\frac{1}{r}\frac{d(rQ_r)}{dr} = \upsilon\dot{w} + \rho_A\ddot{w} \tag{1}$$

and

$$Q_r = \frac{dM_r}{dr} + \frac{M_r - M_\theta}{r}, \tag{2}$$

where Q_r is the transverse shear force resultant, M_r and M_θ are the radial and tangential moment resultants, $\dot{w}$ is the velocity in the axial direction, $\ddot{w}$ is the acceleration in the axial direction, υ is the damping coefficient per unit area, and ρ_A is the areal density given by

$$\rho_A = \int_{-H/2}^{H/2} \rho\, d\bar{z}. \tag{3}$$

Damping in (1) comes from a variety of sources including radiation resistance, thermoelastic dissipation, radiation of bending waves into the supporting structure, etc. The damping coefficient per unit area is related to the classical second-order system damping coefficient, ζ (Bendat and Piersol, 2000), and the natural frequency of an isotropic, clamped, circular plate, ω_n (Leissa, 1993), as follows (Bendat and Piersol, 2000):

$$\upsilon = 2\omega_n\zeta\rho_A. \tag{4}$$

The classical second-order system damping coefficient, ζ, is extracted from experimental data for a device with geometry similar to that given in Table 1 and is shown to be approximately 0.008 (Chandrasekaran et al., 2002). The fundamental natural frequency of an isotropic plate is found in Section 4.

2.2. Kinematic equations

Kirchoff's hypothesis suggests the following displacement field for a circular, axisymmetric plate (Reddy, 1999):

$$w = w_0(r) \quad \text{and} \quad u = u_0(r) - \bar{z}\frac{\partial w_0(r)}{\partial r}, \tag{5}$$

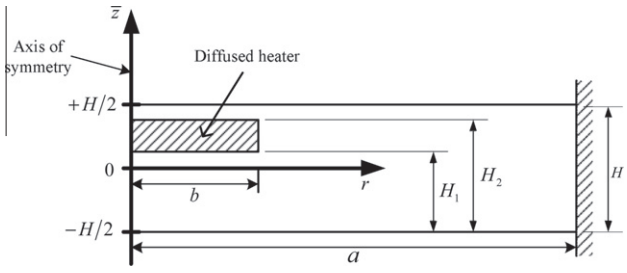

Fig. 2. Axisymmetric, isotropic plate with an internal, diffused heater.

Table 1
Material properties and geometry.

Property	Value
a	500 μm
H	6 μm
H_1	4.5 μm
H_2	5.5 μm
b	30 μm
g_0	14.1 μW/μm^3
α	9.56E−5 m^2/s
κ	1.56E−5 kg mm/K s^3
ρ	2330 kg/m^3
E	150 GPa
ν	0.27
γ	2.6E−6 1/K
ζ	0.008

where w and u are the displacement fields in the vertical and radial directions, respectively, and w_0 and u_0 are the local displacements in the vertical and radial directions, respectively, "at the reference surface", i.e. $\bar{z}=0$. The linear-strain displacement relationships for the axisymmetric plate are (Reddy, 1999):

$$\begin{Bmatrix} \varepsilon_r \\ \varepsilon_\theta \end{Bmatrix} = \begin{Bmatrix} \frac{\partial u}{\partial r} \\ \frac{u}{r} \end{Bmatrix}. \tag{6}$$

Upon substituting the displacement fields given in (5) into (6), the strain equations become

$$\begin{Bmatrix} \varepsilon_r \\ \varepsilon_\theta \end{Bmatrix} = \begin{Bmatrix} \frac{du_0}{dr} - \bar{z}\frac{d^2w_0}{dr^2} \\ \frac{u_0}{r} - \bar{z}\frac{1}{r}\frac{dw_0}{dr} \end{Bmatrix}. \tag{7}$$

2.3. Constitutive relationship

In developing the stress–strain relationships, it is assumed that the material is isotropic. The assumption of isotropic elastic properties for silicon is a simplification based on its moderate degree of anisotropy (Madou, 2002). Ignoring transverse loading, the stress–strain relationship for an axisymmetric plate under thermal loading is defined by Reddy (1999)

$$\begin{Bmatrix} \sigma_r \\ \sigma_\theta \end{Bmatrix} = [Q]\begin{Bmatrix} \varepsilon_r \\ \varepsilon_\theta \end{Bmatrix} - \frac{E\gamma}{1-\nu}\theta(r,\bar{z},t)\begin{Bmatrix} 1 \\ 1 \end{Bmatrix}, \tag{8}$$

where E is the Young's modulus, ν is Poisson's ratio, γ is the coefficient of thermal expansion, θ is the spatially and temporally dependent temperature difference with respect to ambient temperature ($\theta = T - T_\infty$), and [Q] is the stiffness matrix

$$[Q] = \frac{E}{1-\nu^2}\begin{bmatrix} 1 & \nu \\ \nu & 1 \end{bmatrix}. \tag{9}$$

The radial and tangential moments per unit length are

$$\begin{Bmatrix} M_r \\ M_\theta \end{Bmatrix} = \int_{-H/2}^{H/2} \begin{Bmatrix} \sigma_r \\ \sigma_\theta \end{Bmatrix} \bar{z}\, d\bar{z}. \tag{10}$$

Integrating (10) yields

$$\begin{Bmatrix} M_r \\ M_\theta \end{Bmatrix} = -D\begin{bmatrix} 1 & \nu \\ \nu & 1 \end{bmatrix}\begin{Bmatrix} \frac{d^2w_0}{dr^2} \\ \frac{1}{r}\frac{dw_0}{dr} \end{Bmatrix} - \begin{Bmatrix} M^T \\ M^T \end{Bmatrix}, \tag{11}$$

where the thermal moment is (Reddy, 1999)

$$M^T = \int_{-H/2}^{H/2} \frac{E}{1-\nu}\theta(r,\bar{z},t)\gamma\bar{z}\, d\bar{z}. \tag{12}$$

Substituting (11) into (2) gives the shear force per unit length,

$$Q_r = -D\left(\frac{d^3w_0}{dr^3} + \frac{1}{r}\frac{d^2w_0}{dr^2} - \frac{1}{r^2}\frac{dw_0}{dr}\right) - \frac{dM_r^T}{dr}. \tag{13}$$

2.4. Displacement differential equation

To obtain a displacement equation in terms of strictly w_0, (13) is substituted into (1) to obtain (Reddy, 1999):

$$D\nabla^4 w_0 + \upsilon\dot{w}_0 + \rho_A\ddot{w}_0 = -\nabla^2 M^T, \tag{14}$$

where ∇^4 is the axisymmetric biharmonic operator in cylindrical coordinates (Kaplan, 2003). The left hand side of (14) is the bending wave equation while the right hand side serves as the distributed thermal forcing function. The first term on the left accounts for stiffness in the plate. The second and third terms are due to damping and inertia, respectively. The temperature field is needed to calculate the thermal forcing term on the right hand side.

The boundary conditions for a clamped plate are (Leissa, 1993):

$$w_0(r=a) \quad \text{and} \quad \left.\frac{dw_0}{dr}\right|_{r=a} = 0. \tag{15}$$

Also, the displacement and its derivative remain finite at the origin (Leissa, 1993):

$$w_0(r=0) \quad \text{and} \quad \left.\frac{dw_0}{dr}\right|_{r=0} < \infty. \tag{16}$$

Although axisymmetry implies that the deflection slope, $\frac{dw_0}{dr}$, is zero at the plate center, it is shown in Section 4.3 that it is sufficient to impose that the slope remain finite.

3. Temperature solution

A solution of the temperature field from the heat diffusion equation is needed to form the thermal forcing term on the right hand side of (14). The temperature field is independent of the elastic strain rate in the device as long as the time scale of heat transfer is not much greater than the time scale of vibration (Speziale, 2001):

$$t_{ht} \gg \frac{1}{f}, \tag{17}$$

where f is the frequency and the time scale of heat transfer is

$$t_{ht} = \frac{a^2}{\alpha}, \tag{18}$$

where a represents the largest length scale of the structure and α is the thermal diffusivity. Thus, the heat diffusion equation is decoupled when

$$\frac{a^2}{\alpha} f \gg 1. \tag{19}$$

A discussion of the implication of assumption (19) is contained in Section 5.

A circular diaphragm with non-uniform internal heat generation is shown in Fig. 2. The 2-D heat diffusion equation governs temperature distribution in the plate and is written in terms of the temperature difference as Ozisik (1993)

$$\nabla^2\theta + \frac{1}{\kappa}g(r,z,t) = \frac{1}{\alpha}\frac{\partial\theta}{\partial t}, \tag{20}$$

where κ is the thermal conductivity, ∇^2 is the axisymmetric Laplacian, and $g(r,z,t)$ is the internal heat generation function. The heater is assumed to be cylindrical and contained within the plate thickness such that the internal heat generation function becomes

$$g(r,z,t) = g_0[U(r) - U(r-b)] \cdot [U(z-H_1) - U(z-H_2)]\mathrm{Re}[e^{j\omega t}], \quad (21)$$

where $U(x)$ is the unit step function (Kreyszig, 2006) and g_0 is the heat generation amplitude. The formation of the diffused heater is assumed to have no effect on the thermodynamic or elastic properties of the material.

Note, the axial coordinate origin in Fig. 2 used to form the displacement (14) is shifted from the center to the bottom of the plate in (20) and (21), and the rest of the temperature analysis to increase the solution simplicity. The new axial coordinate is referred to as $z = \bar{z} + \frac{H}{2}$.

Eq. (20) is a partial differential equation of second order in space and first order in time requiring four boundary conditions and one initial condition. Assumptions are made to arrive at simple boundary conditions.

First, the thermal diffusion length scale is assumed to be smaller than the radius of the plate so the temperature around the circumference of the diaphragm is maintained at the ambient temperature,

$$\theta(r=a) = 0. \quad (22)$$

This assumption is violated at low frequencies because the diffusion length scales as Ozisik (1993)

$$\lambda_{diff} \propto \sqrt{\frac{\alpha}{\omega}}. \quad (23)$$

Thus, at low frequencies the diffusion length scale will become on the order of the plate radius. The prescribed boundary condition will artificially force the temperature to zero at the plate edge. This will create an erroneously large radial temperature gradient and over-predict the thermal forcing function.

Convective boundary conditions exist between the diaphragm surfaces and the air. The formulation of a convective coefficient on the diaphragm surfaces is non-trivial and markedly increases the complexity of the solution. For simplicity of initial studies, the heat transfer between the air and surfaces of the diaphragm is ignored such that the top and bottom surfaces are assumed to be thermally insulated,

$$\left.\frac{\partial\theta}{\partial z}\right|_{z=0} = \left.\frac{\partial\theta}{\partial z}\right|_{z=H} = 0. \quad (24)$$

The final boundary condition requires a finite temperature difference at the center of the diaphragm,

$$\theta(r \to 0) < \infty. \quad (25)$$

In addition, the initial temperature of the diaphragm is also assumed to be ambient

$$\theta|_{t=0} = 0. \quad (26)$$

A Green's function formulation is used to find the solution to (20). Green's functions are useful for solving non-homogeneous, transient heat conduction problems. The axisymmetric, two-dimensional Green's function represents the temperature at position $\mathbf{r}$ and time t due to a ring heat source of unity strength located at $\mathbf{r}'$ that impulses at time τ. The solution for the temperature difference in terms of Green's functions is (Ozisik, 1993)

$$\theta(\mathbf{r},t) = \int G(\mathbf{r},t|\mathbf{r}',\tau)|_{\tau=0} F(\mathbf{r}')dA' + \frac{\alpha}{\kappa}\int_{\tau=0}^{t}\int g(\mathbf{r}',\tau)G(\mathbf{r},t|\mathbf{r}',\tau)dA'd\tau + \alpha\int_{\tau=0}^{t}\sum_{i=1}^{N}\int G(\mathbf{r},t|\mathbf{r}',\tau)|_{\mathbf{r}'=\mathbf{r}_i}\frac{1}{\kappa_i}f_i dl_i d\tau, \quad (27)$$

where $F(\mathbf{r})$ is the initial condition, N represents the number of boundaries and f_i is extracted from the general boundary condition on the temperature difference,

$$\kappa_i\frac{\partial\theta}{\partial n_i} + h_i\theta = f_i(r,t). \quad (28)$$

The three terms in (27) account for the initial conditions, internal heat generation, and non-homogeneous boundary conditions, respectively. The first and third terms are zero due to the homogeneous boundary conditions and the zero initial condition given in (22)–(26). Thus, (27) simplifies to

$$\theta(\mathbf{r},t) = \frac{\alpha}{\kappa}\int_{\tau=0}^{t}\int g(\mathbf{r}',\tau)G(\mathbf{r},t|\mathbf{r}',\tau)dA'd\tau. \quad (29)$$

The Green's function is found in the following section using a separation of variables technique found in Ozisik (1993).

3.1. Determination of the Green's function

First, the homogeneous form of (20) and boundary conditions (22)–(25) are solved given a general initial condition $F(r,z)$. Then, the solution is compared to (27) and the Green's function at $\tau = 0$ is extracted (Ozisik, 1993). Finally, the full Green's function is found by replacing t by $t - \tau$ (Ozisik, 1993).

The solution to the homogeneous heat conduction problem is

$$\theta_h = \int_0^H\int_0^a F(r',z')\sum_{m=1}^{\infty}\sum_{n=0}^{\infty}\frac{1}{N_{nm}}J_0(\nu_m r')J_0(\nu_m r) \cdot \cos(\eta_n z')\cos(\eta_n z)e^{-\lambda_{nm}^2\alpha t}r'\,dr'\,dz', \quad (30)$$

where the eigenvalues are found from

$$\eta_n = \frac{n\pi}{H}, \quad n = 0,1,2\ldots$$

and

$$J_0(\nu_m a) = 0, \quad m = 1,2,3\ldots$$

and $\lambda_{nm}^2 = \nu_m^2 + \eta_n^2$. Comparing (30) with (29) and replacing t with $t - \tau$, the general Green's function is extracted as

$$G(r,z,t|r',z',\tau) = \sum_{m=1}^{\infty}\sum_{n=0}^{\infty}\frac{1}{N_{nm}}J_0(\nu_m r')J_0(\nu_m r) \cdot \cos(\eta_n z')\cos(\eta_n z)e^{-\lambda_{nm}^2\alpha(t-\tau)}. \quad (31)$$

3.2. Final temperature solution formulation

Substituting the heat generation (21) and the Green's function (31) into (29) and integrating yields

$$\theta(r,z,t) = \mathrm{Re}\left[\frac{2\alpha g_0 b}{\kappa a^2}\sum_{m=1}^{\infty}\frac{1}{\nu_m}\frac{J_1(\nu_m b)J_0(\nu_m r)}{J_1^2(\nu_m a)}\cdot\sum_{n=0}^{\infty}B_n\cos(\eta_n z)\frac{e^{j\omega t} - e^{-\lambda_{nm}^2\alpha t}}{j\omega + \lambda_{nm}^2\alpha}\right], \quad (32)$$

where

$$B_n = \begin{cases} n = 0, & \frac{H_2 - H_1}{H}; \\ n > 0, & \frac{2}{n\pi}\left[\sin\left(n\pi\frac{H_2}{H}\right) - \sin\left(n\pi\frac{H_1}{H}\right)\right]. \end{cases}$$

Note that the solution has a transient term, $e^{-\lambda_{nm}^2\alpha t}$. The transient solution is sensitive to the temperature boundary condition (22) at $r = a$. A mixed boundary condition would provide a more general solution but is not obvious to formulate.

3.3. Steady-state solution

Eliminating transient terms in (32) yields the sinusoidal steady-state solution. It is easily seen that $e^{-\lambda_{mn}^2 \alpha t}$ decays to zero as time progresses. Thus, the steady state solution is

$$\theta(r,z,t) = \mathrm{Re}\left[\frac{2\alpha g_0 b e^{j\omega t}}{\kappa a^2} \cdot \sum_{m=1}^{\infty} \frac{J_1(\nu_m b) J_0(\nu_m r)}{\nu_m J_1^2(\nu_m a)} \sum_{n=0}^{\infty} \frac{B_n \cos(\eta_n z)}{j\omega + \lambda_{nm}^2 \alpha}\right]. \tag{33}$$

4. Displacement solution

Now that the temperature field has been formulated, the solution to the bending wave equation under thermal forcing (14) is found. To find the sinusoidal steady-state solution, the displacement is assumed to have the form

$$w_0 = \mathrm{Re}\left[\bar{w}(r) e^{j\omega t}\right]. \tag{34}$$

Substituting the steady-state temperature solution (33) into (12) and integrating results in the thermal moment,

$$M^T = \frac{E\gamma}{1-\nu} \frac{2\alpha g_0 b H^2}{\kappa \pi^2 a^2} \mathrm{Re}\left[e^{j\omega t} \cdot \sum_{m=1}^{\infty} \frac{J_1(\nu_m b) J_0(\nu_m r)}{\nu_m J_1^2(\nu_m a)} \sum_{n=1}^{\infty} \frac{(-1)^n - 1}{n^2} \frac{B_n}{j\omega + \lambda_{nm}^2 \alpha}\right]. \tag{35}$$

Taking the axisymmetric Laplacian of the thermal moment gives

$$\nabla^2 M^T = \mathrm{Re}\left[e^{j\omega t} \sum_{m=1}^{\infty} J_0(\nu_m r) \varsigma(\nu_m)\right], \tag{36}$$

where

$$\varsigma(\nu_m) = \frac{E\gamma}{1-\nu} \frac{2\alpha g_0 b H^2}{\kappa \pi^2 a^2} \frac{\nu_m J_1(\nu_m b)}{J_1^2(\nu_m a)} \sum_{n=1}^{\infty} \frac{1-(-1)^n}{n^2} \frac{B_n}{j\omega + \lambda_{nm}^2 \alpha}.$$

Substituting (36) into (14) yields

$$\nabla^4 \bar{w} - \frac{1}{D}(\omega^2 \rho_A - j\omega \upsilon)\bar{w} = \frac{1}{D} \sum_{m=1}^{\infty} J_0(\nu_m r) \varsigma(\nu_m). \tag{37}$$

4.1. Homogeneous solution

First, the solution to the homogeneous equation,

$$\nabla^4 \bar{w}_h - \frac{1}{D}(\omega^2 \rho_A - j\omega \upsilon)\bar{w}_h = 0 \tag{38}$$

is found. Factoring (38) results in

$$(\nabla^2 - \chi^2)(\nabla^2 + \chi^2)\bar{w}_h = 0, \tag{39}$$

where

$$\chi^2 = \sqrt{\frac{\omega^2 \rho_A - j\omega \upsilon}{D}}. \tag{40}$$

The complete solution to the homogenous equation is obtained by superimposing the solutions to the equations

$$(\nabla^2 + \chi^2)\bar{w}_{h1} = 0 \tag{41}$$

and

$$(\nabla^2 - \chi^2)\bar{w}_{h2} = 0. \tag{42}$$

These equations are the zeroth order Bessel's equation and Modified Bessel's equation, respectively. Thus, the homogeneous solution is (Leissa, 1993)

$$\bar{w}_h(r) = c_1 J_0(\chi r) + c_2 Y_0(\chi r) + c_3 I_0(\chi r) + c_4 K_0(\chi r). \tag{43}$$

The fundamental natural frequency is found from the homogeneous, undamped solution (Leissa, 1993). After applying (16), the clamped boundary conditions are written in matrix form as

$$\begin{bmatrix} J_0(\chi r) & I_0(\chi r) \\ -\chi J_1(\chi r) & \chi I_1(\chi r) \end{bmatrix} = 0. \tag{44}$$

The fundamental natural frequency is found by taking the determinant of (44) and setting it equal to zero. The result is (Leissa, 1993)

$$\omega_n = \frac{10.2158}{a^2} \sqrt{\frac{D}{\rho_A}}. \tag{45}$$

4.2. Particular solution

The particular solution takes the form of the thermoelastic forcing function on the right hand side of (37),

$$\bar{w}_p(r) = \sum_{m=1}^{\infty} c_5 J_0(\nu_m r). \tag{46}$$

Plugging the particular solution into (37) and solving for c_5,

$$c_5 = \frac{1}{D} \frac{\varsigma(\nu_m)}{\nu_m^4 - \chi^4}. \tag{47}$$

4.3. Final solution

The total solution is given by the summation of the homogeneous and particular solutions,

$$\bar{w}(r) = \sum_{m=1}^{\infty} c_1 J_0(\chi r) + c_2 Y_0(\chi r) + c_3 I_0(\chi r) + c_4 K_0(\chi r) + c_5 J_0(\nu_m r). \tag{48}$$

Applying the finite boundary conditions (16), c_2 and c_4 must be zero (Leissa, 1993). Applying the clamped boundary conditions (15) and solving for the remaining constants in terms of c_5, the final solution is

$$\bar{w}(r) = \sum_{m=1}^{\infty} c_5 [J_0(\nu_m r) + C_m J_0(\chi a) I_0(\chi r) - C_m I_0(\chi a) J_0(\chi r)], \tag{49}$$

where

$$C_m = \frac{\nu_m J_1(\nu_m a)}{\chi I_0(\chi a) J_1(\chi a) + \chi I_1(\chi a) J_0(\chi a)}. \tag{50}$$

5. Results

The material parameters and geometry used to form the results are motivated by a typical MEMS structure (Chandrasekaran et al., 2002) and are outlined in Table 1. The temperature difference, θ, versus the plate radius and thickness are shown in Figs. 3 and 4, respectively, for multiple frequencies. The phases of the temperature differences are referenced to the phases of the maximum temperature difference at the plate center for each frequency. The center deflection frequency response and deflection mode shapes are given in Fig. 5. The phases of the deflection mode shapes are also referred to the phase of the maximum deflection at the plate center for each frequency. In all of the plots, FEA results are provided as verification of the analytical solution. The FEA results were found in COMSOL Multiphysics using the "General Heat Transfer" and "Axial Symmetry, Stress Strain" modules. The structural frequency response analysis was coupled to a frequency domain analysis of the heat transfer equation formed by specifying an internal heat generation equal to $-j\omega\kappa T/\alpha$ in the static heat transfer

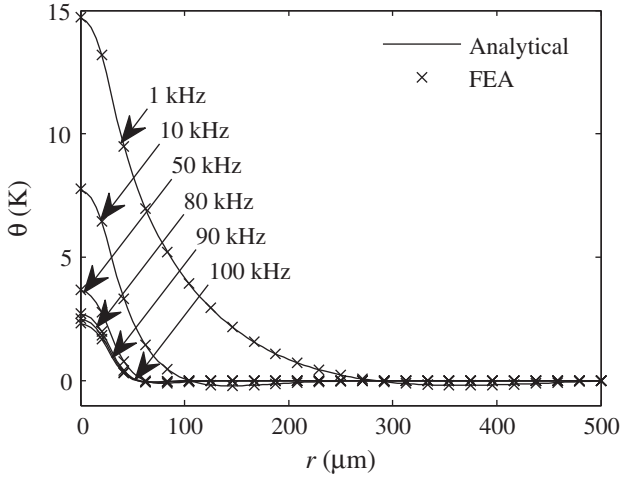

Fig. 3. Temperature variation along the midplane of the diaphragm.

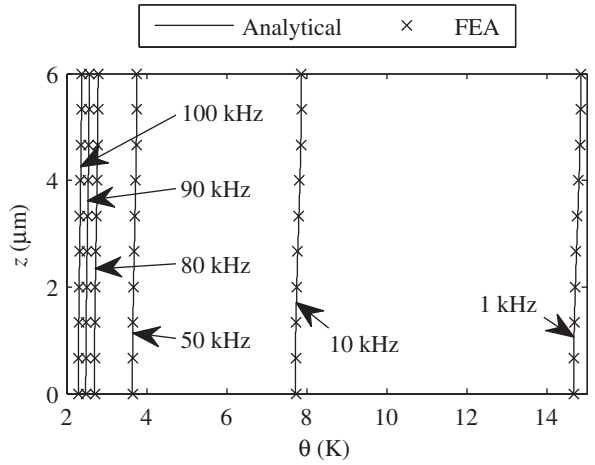

Fig. 4. Temperature variation across the diaphragm.

equation. Vertical deflection of the midplane of the plate was restricted at $r = a$. Radial deflection was also bound at the plate edge. The mesh consisted of 6,144 Lagrange, triangular elements that are linear in temperature and quadratic in stress and strain. The computational time of the analytical solution for a single frequency using Matlab is 96 ± 15 ms on a Dual Core Opteron 64-bit workstation with 12 GB of RAM, which compares favorably to the 6.80 s calculation in COMSOL.

The temperature difference as a function of radius is shown in Fig. 3 for several frequencies. At high frequencies the thermal diffusion length scale is smaller than the diaphragm radius and the temperature difference approaches zero inward of the plate edge. In this case, the zero temperature difference boundary condition at the diaphragm edge (22) is justified. At lower frequencies, the period of oscillation and the thermal time constant become comparable, as do the thermal diffusion length scale and the diaphragm radius, resulting in heat diffusion to the diaphragm edge. The edge boundary condition (22), however, forces the temperature change to zero. Thus, at low frequencies the edge boundary condition has a significant impact on the temperature solution. A mixed boundary condition at the diaphragm edge, such as Ozisik (1993)

$$\kappa \frac{\partial \theta}{\partial r} + h_r \theta = 0, \tag{51}$$

would provide a more accurate representation of the device structure at low frequencies. The constant, h_r, that relates the temperature difference to its gradient, however, is not trivial and may be geometry and/or material dependent.

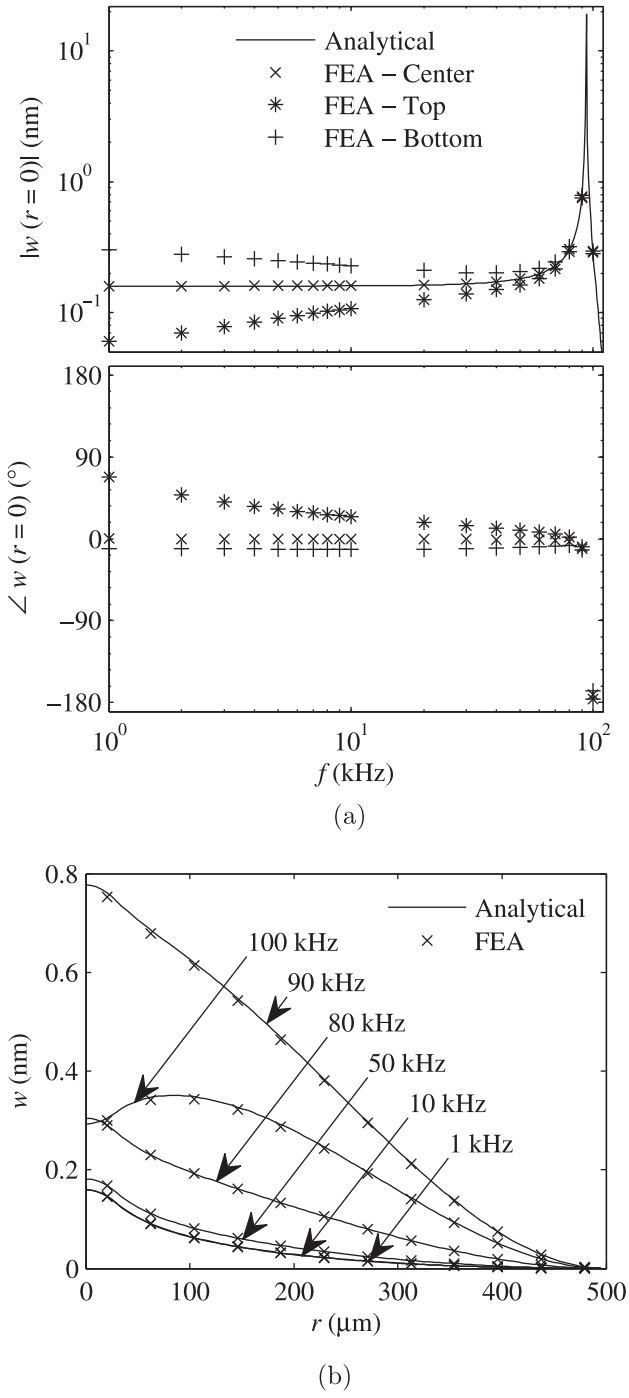

Fig. 5. Coupled thermal-displacement solution.

There is a minor gradient in temperature, θ, between the top and bottom of the plate as shown in Fig. 4 since the thermal diffusion length scale is large in comparison to the thickness of the plate for the frequencies studied. The temperature decreases at higher frequencies where the period of oscillation is less than the thermal time constant and there is not enough time for heat diffusion to occur.

The frequency response of the center deflection is shown in Fig. 5a. The resonance is seen to occur at approximately 94 kHz. Mode shapes of the deflection of the center of the plate in the flat-band and near the resonant frequency are shown in Fig. 5b. At

100 kHz, just beyond the first resonance, the mode shape displays second radial mode behavior. Note that the classical second-order system damping coefficient, $\zeta = 0.008$, is extracted from experimental data (Chandrasekaran et al., 2002) and shapes the width and height of the resonant peak.

Also shown in Fig. 5a are the magnitude and phase of the center deflections of the top, middle, and bottom surfaces of the plate calculated using FEA. It is interesting to note that at frequencies lower than resonance, there are significant differences in deflection between the top and bottom surfaces, which indicates the significance of thermal expansion at the radial center of the plate where the heater is located. After first examination, one might suspect that this is a residual of the temperature boundary condition at the diaphragm radius. Upon further inspection, the thermal expansion is significant at frequencies where the radial temperature boundary condition is justified. For example, at 50 kHz, the thermal expansion is still significant in Fig. 5a while the thermal diffusion length scale is clearly less than the diaphragm radius in Fig. 3. In Fig. 6 the phase locked deflections of the top, middle, and bottom surfaces of the plate are shown at 10 and 50 kHz. Clearly, in Fig. 6b, the effect of the thermal expansion is isolated to the region around the heater. Fig. 6b shows a more significant thermal expansion effect at a forcing frequency of 1 kHz. As previously discussed in Section 3, however, the temperature boundary condition at the diaphragm radius at 1 kHz is violated. In addition, significant thermal expansion of the thickness of the diaphragm is a direct violation of classical plate theory that assumes the strain in the transverse direction of the plate to be negligible. Clearly, a higher order thermomechanical analytical model would be needed to capture the affects of thermal expansion away from resonance.

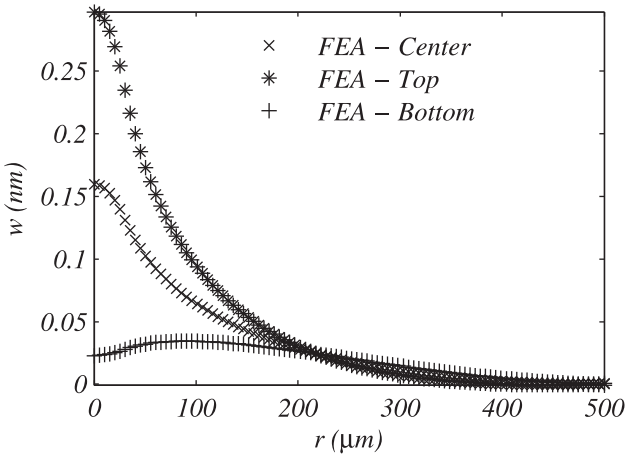

(a) 1 kHz

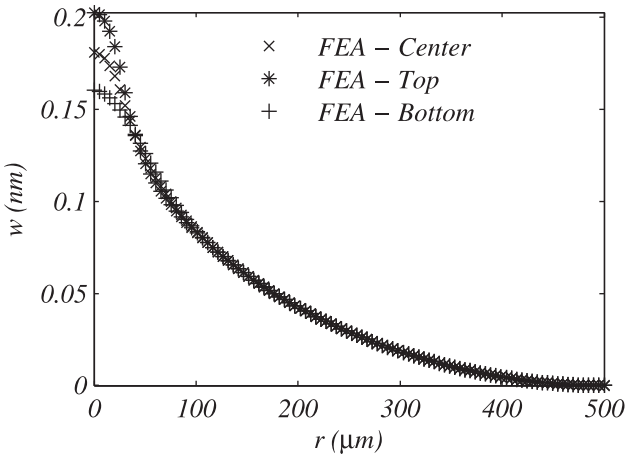

(b) 50 kHz

Fig. 6. FEA results of the coupled thermal-displacement model.

6. Conclusions

An analytical model for thermoelastic actuation of an isotropic, circular plate has been developed. The analytical solutions of the bending wave and heat conduction equations were found. First, the bending wave equation under thermal forcing was derived. Then, the temperature field created by an internal heater was determined using a Green's function formulation. The resulting temperature field was applied as the thermal forcing term in the bending wave equation. Comparison of the analytic and finite element results shows excellent agreement. The analytical solution has considerably lower computational costs, making it suitable for design optimization.

Future work on the modeling of this device will include composite layers, the impact of fabrication induced in-plane residual stress, and further investigate thermal expansion as a significant contributor to mechanical deflection. The results will be compared to laser vibrometer measurements of an existing thermoelastic MEMS.

Acknowledgements

This material is based on work supported under two National Science Foundation Graduate Fellowships as well as the Office of Naval Research (contract #N00014-00-1-0343) monitored by Dr. Kam Ng. The authors also acknowledge Dr. David Hahn for his assistance with the thermal analysis.

References

Bendat, J.S., Piersol, A.G., 2000. Random Data: Analysis and Measurement Procedures, third ed.. Wiley Series in Probability and Statistics Wiley, New York.

Brand, O., Hornung, M.R., Baltes, H., Hafner, C., 1997. Ultrasound barrier microsystem for object detection based on micromachined transducer elements. IEEE J. Microelectromech. S. 6 (2), 151–160.

Campbell, S.A., 2001. The Science and Engineering of Microelectronic Fabrication, second ed.. The Oxford Series in Electrical and Computer Engineering Oxford University Press.

Chandrasekaran, V., Chow, E.M., Kenny, T.W., Nishida, T., Sankar, B.V., Cattafesta, L.N., Sheplak, M., 2002. Thermoelastically actuated acoustic proximity sensor with integrated electrical through-wafer interconnects. In: Technical digest Sensor and Actuator Workshop. Hilton Head, SC, pp. 102–106.

Chandrasekaran, V., Sankar, B.V., Cattafesta, L.N., Nishida, T., Sheplak, M., 2003. An analytical model for the thermoelastic actuation of composite diaphragms. In: 12th International Conference on Transducers, Solid-State Sensors, Actuators and Microsystems, vol. 2, pp. 1844–1847.

Hornung, M.R., Brand, O., 1999. Micromachined Ultrasound-based Proximity Sensors. Kluwer Academic, Boston.

Irie, T., Yamada, G., 1978. Thermally induced vibration of circular plate. Bull. Jpn. Soc. Mech. Eng. 21 (162), 1703–1709.

Kaplan, W., 2003. Advanced Calculus, fifth ed. Addison-Wesley, Boston.

Kreyszig, E., 2006. Advanced Engineering Mathematics, ninth ed. John Wiley, Hoboken, NJ.

Lammerink, T.S.J., Elwenspoek, M., Fluitman, J.H.J., 1991. Frequency-dependence of thermal excitation of micromechanical resonators. Sens. Actuators, A 27 (1–3), 685–689.

Lammerink, T.S.J., Elwenspoek, M., Fluitman, J.H.J., 1992. Thermal actuation of clamped silicon microbeams. Sens. Mater. 3, 217–238.

Lammerink, T.S.J., Elwenspoek, M., Vanouwerkerk, R.H., Bouwstra, S., Fluitman, J.H.J., 1990. Performance of thermally excited resonators. Sens. Actuators, A 21 (1–3), 352–356.

Leissa, A.W., 1993. Vibration of Plates, reprinted ed. Acoustical Society of America through the American Institute of Physics.

Madou, M.J., 2002. Fundamentals of Microfabrication: The Science of Miniaturization, second ed. CRC Press, Boca Raton.

Ozisik, M.N., 1993. Heat Conduction, second ed. John Wiley & Sons, Inc., New York.

Paul, O., Baltes, H., 1999. Mechanical behavior and sound generation efficiency of prestressed, elastically clamped and thermomechanically driven thin film sandwiches. J. Micromech. Microeng. 9 (1), 19–29.
Popescu, D.S., Dascalu, D.C., Elwenspoek, M., Lammerink, T., 1996. Ultrasonic transducer with thermomechanical excitation and piezoresistive detection. Semiconductor Conference, International, vol. 1. IEEE, pp. 85–88.
Prasanna, S., Spearing, S.M., 2007. Materials selection and design of microelectrothermal bimaterial actuators. IEEE J. Microelectromech. S. 16 (2), 248–259.
Reddy, J.N., 1999. Theory and Analysis of Elastic Plates. Taylor & Francis, Philadelphia.
Rufer, L., Domingues, C.C., Mir, S., Petrini, V., Jeannot, J.C., Delobelle, P., 2006. A cmos compatible ultrasonic transducer fabricated with deep reactive ion etching. IEEE J. Microelectromech. S. 15 (6), 1766–1776.
Speziale, C.G., 2001. On the coupled heat equation of linear thermoelasticity. Acta Mech. 150 (1-2), 121–126.